Mechanical and tribological properties of aluminium incorporated with amorphous Ni$_{60}$Nb$_{40}$ particles

Subramanian Jayalakshmi[a], Ramachandra Arvind Singh[a*], Sanjay Mohan[b], Xizhang Chen[a] & Manoj Gupta[c]

[a]College of Mechanical and Electrical Engineering, Wenzhou University, Wenzhou 325 035, China

[b]School of Mechanical Engineering, Shri Mata Vaishno Devi University, Kakryal, Katra 182 320, Jammu & Kashmir, India

[c]Department of Mechanical Engineering, 9 Engineering Drive 1, National University of Singapore (NUS), Singapore 117 576

In this paper, development and characterization of pure aluminium (Al) reinforced with metallic amorphous Ni$_{60}$Nb$_{40}$ particles has been presented. Ni$_{60}$Nb$_{40}$ amorphous alloy reinforcement powder has been incorporated within Al-metal powder to produce Al-Ni$_{60}$Nb$_{40}$ composite. The composite has been sintered using bidirectional microwave sintering technique. Structure, indentation/tensile/compressive behaviour and tribological properties of the produced Al-10% Ni$_{60}$Nb$_{40}$ have been evaluated. It has been found that the: (i) reinforcement have retained the amorphous structure, (ii) reinforcement have distributed uniformly in the matrix and (iii) interface between the Al-matrix and the amorphous reinforcement has been free of reactive products. Upon comparison of mechanical properties with pure aluminium, the synthesized composite has showed significant enhancement in microhardness, tensile and compressive yield strengths. Under dry sliding wear condition, the composite has showed lower wear rates and lower coefficient of friction. The observed improvement in the composite behaviour has been explained using the processing-microstructure-mechanical properties correlation.

Keywords: Aluminium composites, Glassy reinforcement, Microwave processing, Microstructure, Mechanical behaviour, Tribology

1 Introduction

Aluminium metal matrix composites (Al-MMCs) are promising materials for aeronautical and automotive industries, due to their light-weight and strength properties[1,2]. When compared to monolithic aluminium, Al-MMCs incorporated with ceramic reinforcements such as SiC, Si$_3$N$_4$, Al$_2$O$_3$, SiO$_2$, *etc.,* (in the form of particles, fibres, whiskers) increases the stiffness, strength, hardness, wear resistance and thermal stability. In a recent study[3], it was demonstrated that when LM25 aluminium alloy was incorporated with SiO$_2$ using stir casting method, enhancement in the tensile yield strength ~75% was observed. Similarly, fly ash particle reinforced Al-Si alloy by sintering[4] exhibited ~30% increase in hardness. However, issues such as, (i) undesirable interfacial reactions between matrix and reinforcement, (ii) low ductility and (iii) non-wetting nature of ceramic reinforcement with matrix[1] undermine the performance of Al-MMCs and have thus limited their use in real-time applications. A promising approach to overcome these issues is to consider alternative reinforcements, which are non-ceramic in nature.

Given this scenario, metallic glasses are a prospective alternative. These are advanced materials with lack of long-range periodicity of arrangement of atoms, *i.e.* they do not have grains/grain boundaries[3]. They have thermal properties similar to oxide glasses, *i.e.* they show temperature of glass transition and temperature of crystallization. Owing to these unique properties, these materials exhibit high strength (~2 GPa), large elastic strain (~2%) and excellent corrosion resistance[5]. Further, as these materials are in nature metallic, they can promote improved properties at the interface when reinforced in Al-matrix[6].

Lee and co-workers[7] synthesized Al-composites incorporated Ni-based glassy ribbons by infiltration process and reported twenty five percent compression strength increase. Pure Al and brass matrices containing Ni-/Zr-BMG particles of high-volume fraction were prepared using powder process and were reported[8,9]. When compared to unreinforced material, 60-90% improvement in compression strength was reported. When Mg-matrix and Al-matrix, were incorporated with zirconium, copper and iron amorphous alloys using induction heating method[10-12], significant increase in compression strength properties

were reported. It was observed that the fabrication technique adopted in these works posed limitation on the final dimension of the produced MMC materials (was less than ten millimetre in diameter) to retain the amorphicity. Hence, these works to report only the compressive properties (as small cylindrical samples are sufficient to conduct compression test).

Among the synthesizing methods using powder metallurgy technology, microwave assisted rapid sintering route offer numerous advantages[13]. In the microwave sintering technique, bi-directional heating is used to process the materials[13], due to which temperatures ~823 K to 873 K can be achieved in very less time and dense products of relatively larger dimensions can be made[13,14]. Several pioneering works[15,16] have been reported on this topic. Detailed information on the various processing methods used to synthesize amorphous alloy reinforced light metal composites can be found in literature[17-19].

In this work, microwave sintering was used to synthesize Al-$Ni_{60}Nb_{40}$ composite. The synthesized composite was studied for microstructural, mechanical and wear/friction behaviour and the properties are discussed based on processing-microstructure-mechanical properties correlation.

2 Experimental methods

2.1 Synthesis and characterization of glassy powder

Elemental Ni and Nb metal powder were used to prepare $Ni_{60}Nb_{40}$ (at. %) glassy powder particles, by mechanical alloying technique. The milling process was performed at 300 K, in air (milling time: 87 hours). The ratio of ball and powder was maintained at 3:1 during the milling process and the milling speed was maintained at two hundred revolutions per minute. The phase characteristics of the synthesized glassy powder were investigated by an x-ray diffractometer (XRD, Shimadzu LAB-XRD-6000, copper K-alpha target; wavelength: 1.54056 angstrom) and a scanning electron microscope (Hitachi FESEM-S4300). The thermal characteristics of the amorphous alloy particles were studied using a differential scanning calorimeter (DSC, Perkin-Elmer).

2.2 Synthesis of Al-based Composites

In order to synthesize the aluminium metal matrix composite, elemental Al-powder (having purity of 99.6%) of required quantity was blended with 10% Vf of $Ni_{60}Nb_{40}$ powder for 60 minutes and the powder consolidation was carried out at ambient temperature (cold compacted) at 450 MPa for 60 seconds. The

sintering of the cold-compacted cylindrical billets (diameter: 36 mm) was conducted using a microwave at full power level (*i.e.* 100%) for 750 seconds in order to reach a temperature of 823 K (temperature-time profile was previously calibrated). The billets after sintering, were heated/soaked to 673 K for a time period of 60 minutes. The pre-soaked billets were then extruded at high temperature (623 K), at an applied extrusion pressure of 500 MPa (extrusion ratio: 20.25:1). The extruded rods were 8 mm in diameter.

2.3 Materials Testing and Analysis

2.3.1 X-ray diffraction studies (XRD)

X-ray diffraction analysis was performed on samples cut from the extruded rods and after prior polishing of the samples. An automated Shimadzu LAB-XRD-6000 x-ray diffractometer (Cu, $K\alpha$= 1.54056 Å) was used. Identification of the phases present was conducted by correlating/matching the Bragg angle and peak intensities of the obtained peaks, with those of the standard peaks of elemental aluminium, nickel, niobium and associated chemical products.

2.3.2 Microstructure

Microstructure analysis of the developed composite was performed on the extruded samples taken from the developed amorphous particle reinforced pure Al-matrix composite. The distribution of particles and the intermetallic phase formation (if any) was examined and identified using FESEM. The average size of the amorphous alloy particles was measured using a Scion image analysis software.

2.3.3 Mechanical properties

Cylindrical samples of 8 mm diameter and height 5-7 mm was cut from the extruded Al-materials and were carefully polished to obtain flat parallel surfaces, that are free from scratches. The as-polished samples were used as test samples for measuring microhardenss. Shimadzu HMV automatic digital microhardness tester with a Vickers indenter was used for this purpose. Test were carried out at a load of 0.245 N and a dwell period of 15 seconds. The tests were conducted on 3 samples so as to obtain 10-15 similar, repeatable readings on each sample. Strength properties of the developed Al-composite was conducted under uniaxial tensile loading and compression loading test conditions. The experiments were conducted in a Materials Test System (MTS 810) at ambient

temperature (ASTM:E8M-96). For both tension and compression tests, a crosshead speed of 0.254 mm/min was used. Specimens tested under tension were prepared with 5 mm diameter and 25 mm gauge length. For tests under compression loading, cylindrical samples were prepared with length/ diameter: 1.5. Both tension and compression tests were conducted on a minimum of 5 samples in order to achieve repeatable values. Fractographic studies of the tensile and compression tested samples were investigated using FESEM and the mechanism resulting in fracture was identified.

2.3.4 Wear and friction properties

Dry sliding wear tests were conducted at room temperature (300 K) using a pin-on-disc configuration (Magnum Engineers, Bangalore), at the constant sliding speed of 1 ms-1, with test loads in the range of 10 to 70 N. Cylindrical test specimens made from the Al-composite were of 6 mm in diameter. A hardened EN31steel (62 HRc, with Ra: 30 microns) was used a counterface disc material for the sliding wear tests. Wear was measured as loss in height of the sample due to sliding. A LVDT (range: two thousand micrometer; resolution: 1 micrometer) was incorporated in the machine by design, and was used to measure the height loss. Frictional force was measured using a load cell. To ensure repeatability of test results, three tests were conducted. Both the loss in height and the force due to friction were recorded with respect to the total distance slid. Estimation of wear rate (mm^3/m) and friction coefficient were made from the recorded test data. The worn surface of pure aluminium and the composite due to sliding wear was carried put in a FESEM and the mechanisms of wear was identified.

3 Results and Discussion

3.1 Structure and thermal characteristics of glassy particles

XRD pattern (Fig. 1a) shows the amorphization of elemental Ni and Nb powder of composition $Ni_{60}Nb_{40}$ (at. %) due to ball-milling. The distinct crystalline peaks of the raw materials (Ni and Nb) show a gradual transformation into amorphous phase as identified by the occurrence of halo, typical of amorphous alloys. As seen from the x-ray diffraction curve, such an occurrence is seen with increase in the ball-milling time, indicating the amorphization of the crystalline powder. This observation confirms the transformation of the crystalline state-to-amorphous state of the synthesized powder. The value of the peak position of the amorphous halo occur at 42.84°.

By using Scherrer equation[20], the full-width at half maximum (HWHM) was used to calculate the effective crystallite size and the value is 27 Å (< 3 nm), which supports the observation the structure has been transformed into amorphous state. From the DSC pattern (not shown here)[15,16], the $Ni_{60}Nb_{40}$ amorphous powder showed a crystallization onset temperature (Tx-onset) of 878 K and peak crystallization temperature (Tx-peak) of 930 K. From Fig. 1b, it is seen that the particles have a mean diameter of 10 μm.

3.2 Macroscopic Features of Unreinforced Aluminium Al-$Ni_{60}Nb_{40}$Composite

The visual observation of synthesized pure Al and Al-10% V_f $Ni_{60}Nb_{40}$ composite were free of macroscopic defects. The composite was observed for surface defects and found to be relatively smooth and pore-free. The sintering process parameters such as: (i) relatively high temperature during sintering and (ii) notably shorter time period of holding at that sintering temperature, was achieved successfully by the use
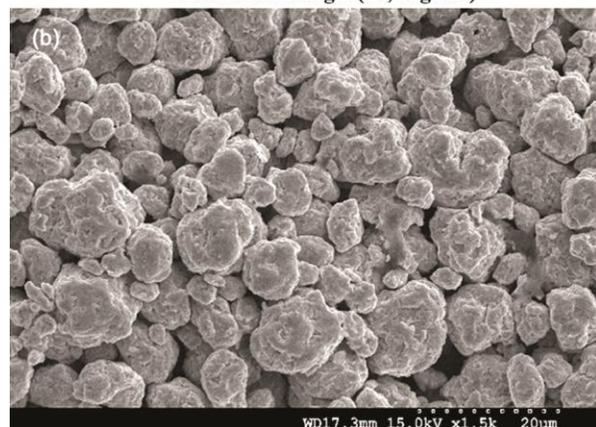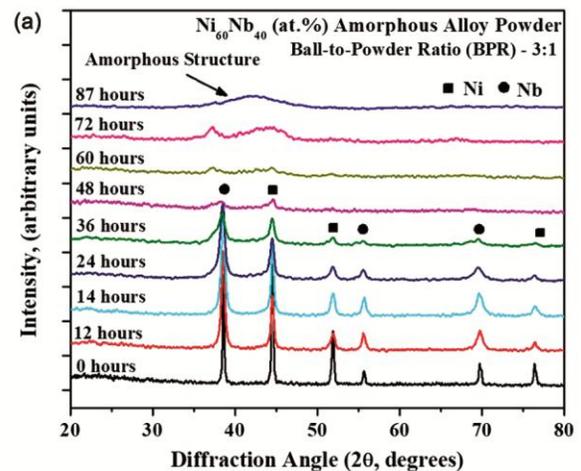
Fig. 1 — (a) Results of diffractogram of nickel and niobium and (b) FESEM pictures of the synthesized $Ni_{60}Nb_{40}$ glassy material.

of bi-direction microwave-assisted rapid sintering process. These parameters were effective in rendering the synthesized composite to have a densely packed structure (*i.e.* with less porosity).

3.3 Microstructural Characterization

3.3.1 X-ray diffraction analyses

Figure 2a shows the diffraction patterns of the synthesized materials from which the following are observed: (i) crystalline peak of elemental Al identified, and crystalline peaks corresponding to any other element or phases were not seen and (ii) the presence of halo that is typical of amorphous structure, which in this case is due to the presence of the reinforced $Ni_{60}Nb_{40}$ powder particles. Also, it can be seen that the position of halo has not been shifted and no peaks of any other phases are present. These observations show that the lack of long-range atomic periodicity existed and crystallinity was not restored, even after conducting sintering at relatively high temperature followed by hot-extrusion. This clearly indicates that reaction between aluminium matrix and the amorphous/glassy reinforcement powder has not occurred, although the microwave sintering process

gives rise to high temperature close to the melting point of aluminium matrix.

To note, if the same Al-amorphous alloy/glassy particle reinforced composite had been synthesized by traditional sintering routes, the process would have to be conducted for longer time period (for uniform and complete sintering). Such longer exposure time between matrix and the reinforcement would have resulted in possible devitrification of the amorphous phase and/or formation of new phases due to interaction between elemental Al, Ni and Nb (such as Al_2Ni and Al_2Nb phases), although Ni-based amorphous alloys have high glass transition temperatures, (Tx-onset) >823 K^{15}. Hence, in the present case, upon microwave sintering, the amorphous state was retained owing to the short time period required for sintering. Consequently, brittle intermetallic phase formation is prevented, which is the major advantage of microwave is sintering when compared to conventional powder-sintering/ solidification routes.

3.3.2 Reinforcement distribution

Figure 2 (b&c) show scanning electron micrographs of Al-$Ni_{60}Nb_{40}$ MMC. Figure 2b shows that the reinforcement distribution is uniform without any
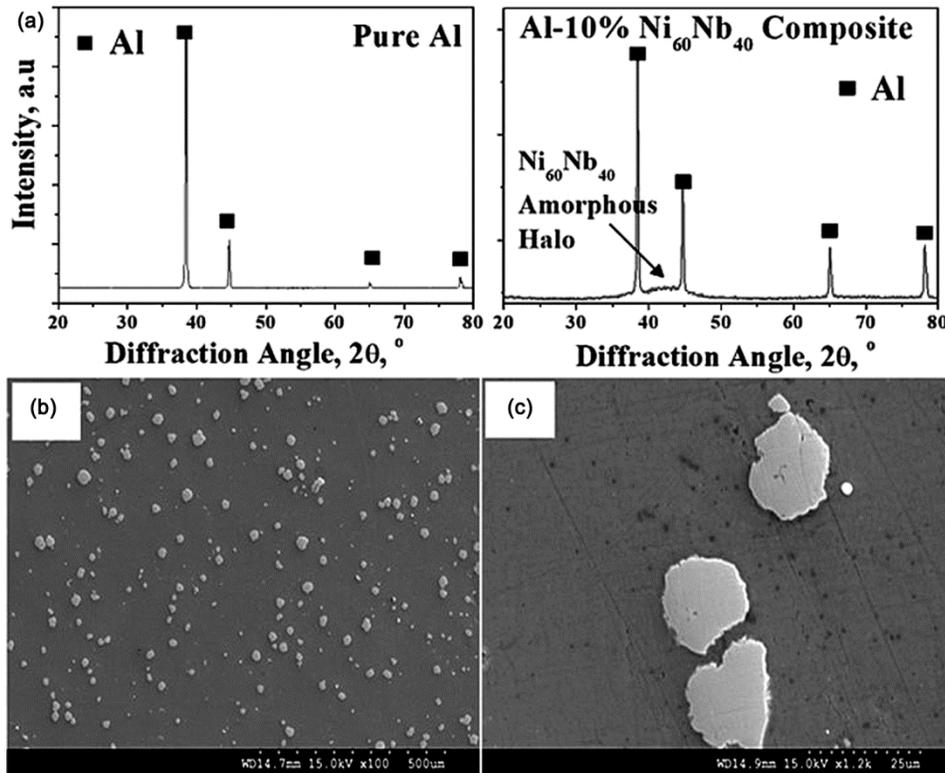
Fig. 2 — (a) Results of diffractogram of unreinforced aluminium and Al-$Ni_{60}Nb_{40}$ composite; (b) SEM pictures showing dispersion of $Ni_{60}Nb_{40}$ particles and (c) SEM pictures showing absence of reaction products at the interface in Al-10%V_f $Ni_{60}Nb_{40}$ amorphous alloy particle reinforced composite.

agglomeration/particle-clustering. Also, even after hot extrusion, amorphous reinforcement particles have retained their near-spherical morphology (*i.e.* the length-to-diameter ratio of ~1 has been retained), indicating that they have not undergone breakage during the secondary processing of extrusion. Figure 2c shows the particle interface at a higher magnification. From this figure, it could be observed that the interface bonding between matrix/ reinforcement particle is good. The absence of reaction products at the interface provides further evidence with regard to the features observed in the x-ray diffractogram (*i.e.* absence of any other phase other than the crystalline peak of aluminium).

3.3.3 Mechanical properties

Table 1 lists the microhardness values of pure Al-matrix and the Al-$Ni_{60}Nb_{40}$ composite. When the microhardness of pure Al is compared to that of the developed composite, a significant increase (~57% increment) in the average value of hardness of the composite was observed. This increase in hardness in the composite is attributed to the inherent high hardness (measured value: 840±40 Hv) of the amorphous alloy particles. During indentation hardness, the amorphous alloy particle reinforcement due to their high inherent hardness, act as hard obstacles and restrict localized deformation of the Al-matrix. This contributes to enhanced work-hardening of the matrix, eventually increasing the microhardness of the developed composite. An earlier work[7] on pure Al-matrix composite reinforced with 20% Ni-base glassy ribbon (with thickness of the order of few tens of micrometer) reported microhardenss value of ~750±40 Hv, which is relatively high, when compared to that of unreinforced aluminium. As is seen in the present work, it demonstrates that the intrinsic high hardness of the particle result in increased composite hardness.

The tensile and compression properties of the synthesized materials are presented in Table 1 and Table 2. Figure 3 (a&b) show the tensile and compression test graphs of the synthesized materials under tensile and compressive loading, respectively.

Table 1 — Results of microhardness and tensile properties of unreinforced aluminium and Al-10% V_f $Ni_{60}Nb_{40}$ composite.

Material	Micro-hardness (H_v)	0.2 % Yield Strength (MPa)	Tensile properties	
			Ultimate Tensile Strength (MPa)	Elongation (%)
Unreinforced Aluminium	53.8 ± 1.7	50 ± 9	65 ± 3	18.5 ± 4.0
Al-10% V_f $Ni_{60}Nb_{40}$	84.5 ± 5.8	60 ± 3	80 ± 6	16.3 ± 0.5

Table 2 — Results of compressive properties of unreinforced aluminium and Al-10%$V_f$$Ni_{60}Nb_{40}$composite.

Material	Compressive properties		
	0.2 % Yield Strength (MPa)	Ultimate Compressive Strength (MPa)	Ductility (%)
Unreinforced Aluminium	80 ± 3	245 ± 6	> 50%
Al-10% V_f $Ni_{60}Nb_{40}$	120 ± 4	310 ± 8	> 50%
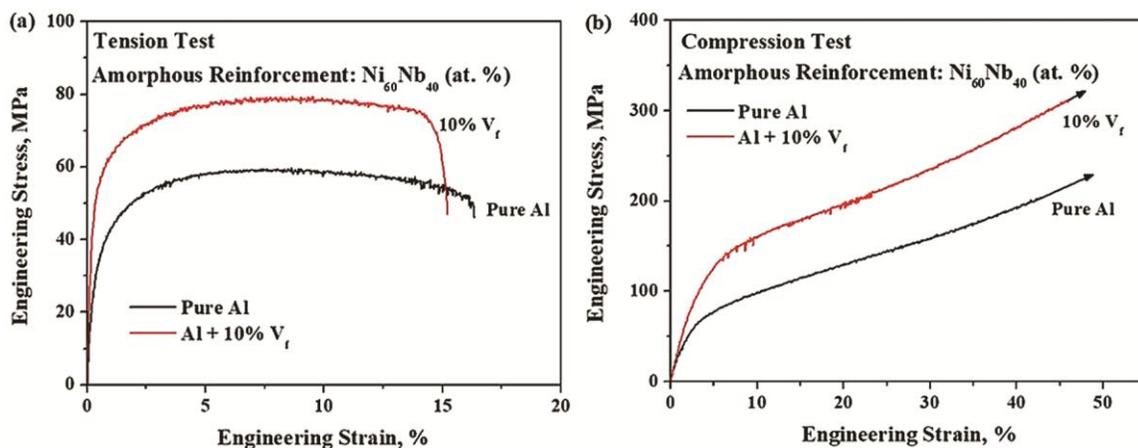
Fig. 3 — (a) Test curves of unreinforced aluminium and Al-$Ni_{60}Nb_{40}$ composite under tensile loading and (b) Test curves of unreinforced aluminium and Al-$Ni_{60}Nb_{40}$ composite under compressive loading.

Under tensile loading (Table 1 and Fig. 3a), the addition of 10 % V_f $Ni_{60}Nb_{40}$ metallic amorphous alloy/glassy particles to pure Al results in increment in strength properties, and a very less reduction in % elongation to failure when compared to those values obtained for pure Al. Such a behaviour is in contrast to those usually observed in composites with conventional ceramic reinforcements, wherein the ceramic reinforcements usually render the composite materials to become very brittle, with little or no plastic deformation[17] (*i.e.* low % elongation values). The compression test data (Table 2 and Fig. 3b) indicate a significant enhancement in yield strength in the composite obtained due to the incorporation of the amorphous alloy reinforcement. On a comparative performance with that of unreinforced aluminium, the Al-$Ni_{60}Nb_{40}$ exhibit almost fifty percent increase in yield stress. Interestingly, the synthesized composite did not undergo fracture under compression even when the strain was 50%. This observation is similar to that of pure Al, which indicates high compressive ductility of the composite. The limiting strain of the compressive tests were ~45-50 %, which is due to the limitation in the equipment.

In MMCs, usually the reinforcement particles act as major load bearing members and it is considered to be the main reason for the enhancement of composite strength properties. The reinforcement (usually ceramics) inherently has high strength, and hence will efficiently carry the load delivered to them by the matrix)[5]. Considering the current work, the amorphous alloy particle reinforcement intrinsically has high strength (for example, Ni-BMG has > 2 GPa strength under compressive loads)[17]. Such intrinsic high strength when used as the reinforcement will effectively carry the load and thereby significantly increase the strength of the composite. Further, the harder $Ni_{60}Nb_{40}$ particles will strengthen the base-matrix[5] via:

a. Orowan strengthening: When moving dislocations comes across hard reinforcement particles, the hard $Ni_{60}Nb_{40}$ particles act as obstacles to motion of dislocation, and causes dislocation to bend across obstacles (dislocation bowing), thereby resulting in the requirement of higher stress to overcome the particle barriers.

b. Owing to the mismatch in yield response between ductile aluminium and hard $Ni_{60}Nb_{40}$, in order to accommodate for the mismatch, geometrically necessary dislocations (GND) are generated that would increase the overall strength of the composite.

c. Aluminium matrix and $Ni_{60}Nb_{40}$ particles have different expansion coefficients, which gives rise to thermal mismatch, that would increase the density of dislocations[21,22]. Such a mismatch (though less when compared to ceramic reinforcement due to its very low CTE) would give rise to local plasticity in the softer aluminium matrix surrounding $Ni_{60}Nb_{40}$, thereby contributing to strengthening effect due to enhancement in the density of dislocations[9].

It is remarkable to note that compressive plastic strain in Al-$Ni_{60}Nb_{40}$ has been retained, and that only a slight decrease in ductility under tensile loading is observed. Retention of ductility in the Al-$Ni_{60}Nb_{40}$ composite is due to the superior elastic strain limit (~2%) of the $Ni_{60}Nb_{40}$ particles, which is unique to metallic amorphous/glassy materials. In conventional MMCs that have ceramic particle reinforcements, the composites exhibit poor ductility owing to the low fracture strain of the ceramic particles[23].

Figure 4 shows tensile fracture surfaces of pure Al and Al-$Ni_{60}Nb_{40}$ composite. Pure Al show extensive ductile failure, typical of aluminium (Fig. 4a). Al-$Ni_{60}Nb_{40}$ composite exhibits dimple morphology and the $Ni_{60}Nb_{40}$ particles are seen within the aluminium matrix (Fig. 4b). Figure 4c shows a higher magnification image of fracture surface of Al-$Ni_{60}Nb_{40}$ composite. From the figure, it is seen that the interface of aluminium/$Ni_{60}Nb_{40}$ is good (arrows), with no particle debonding or particle cracking, indicating efficient transfer of load from the ductile matrix to the particles. Under compression, both unreinforced aluminium and Al-$Ni_{60}Nb_{40}$ exhibited excellent compressive ductility.

3.3.4 Wear and friction properties

Figure 5(a &b) shows the rate of material loss (volume loss) and friction coefficient of unreinforced aluminium and Al-$Ni_{60}Nb_{40}$ composite at varying applied normal loads. The wear rate showed an increasing trend when the applied load was increased for both pure Al and its composite. Wear rate decreased in Al-$Ni_{60}Nb_{40}$ when compared to pure Al, at all the tested loads. Also, when the test load was increased, friction coefficient of the test materials decreased.

The $Ni_{60}Nb_{40}$ amorphous alloy particle composite has better wear resistance than pure Al. The wear behaviour of the test samples follows the Archard's wear equation, which states that the wear of a material is inversely related to its hardness[24]. From the results, it could be inferred that when compared to unreinforced
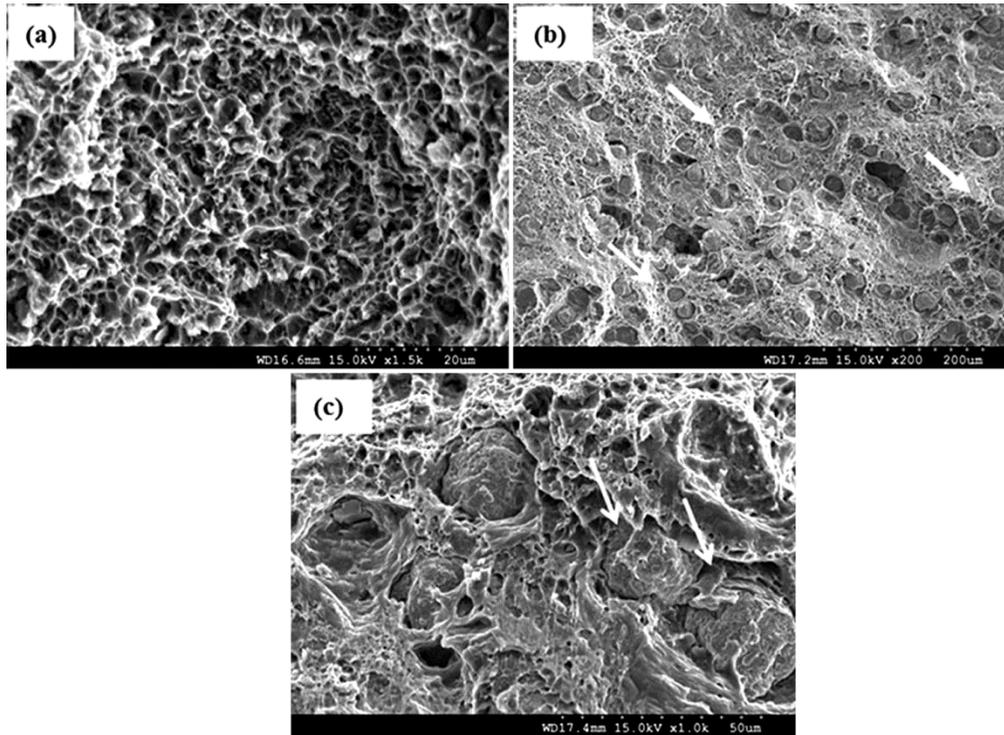
Fig. 4 —Tensile fractographs showing (a) dominant ductile morphology in pure Al, (b) Ductile fracture in Al-10%V_fNi$_{60}$Nb$_{40}$ amorphous alloy particle reinforced composite and (c) Good interface (arrows) with no particle debonding or particle fracture in the Al-10% V_f Ni$_{60}$Nb$_{40}$ composite.
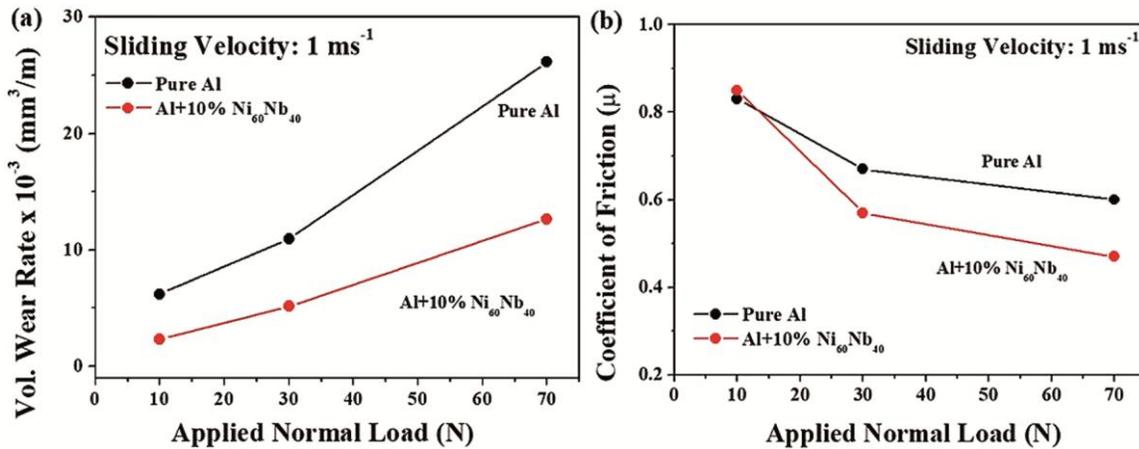
Fig. 5 — (a) Volumetric wear rate versus applied normal load for pure Al and Al-10%V_f Ni$_{60}$Nb$_{40}$ composite and (b) Coefficient of friction versus applied normal load, for pure Al and Al-10% V_f Ni$_{60}$Nb$_{40}$ composite.

aluminium, Al-Ni$_{60}$Nb$_{40}$ composite showed higher wear resistance owing to the composite containing amorphous reinforcement being inherently hard.

The friction coefficient of unreinforced aluminium as well as Al-Ni$_{60}$Nb$_{40}$ composite decreased, when the load was increased, owing to plastic flow of the matrix (the pin material gets extruded at the trailing edge of the pin). Usually, with increase in load, temperature at

the sliding interface increases and causes flow softening of the matrix that leads to lowering of friction[25]. At higher loads, pure Al has higher friction coefficient, whereas the coefficient of friction of amorphous alloy particle reinforced composite is lower. This is due to the lowering of the adhesion component of friction. The reduction in adhesion component of the two sliding surfaces is because of
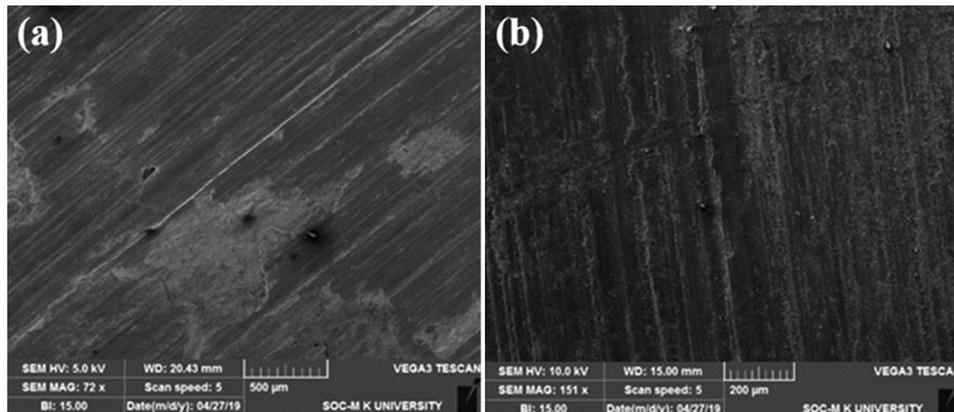
Fig. 6 — Worn surfaces showing (a) Adhesion in pure Al (70 N) and (b) Abrasion in Al-10% V_f $Ni_{60}Nb_{40}$ amorphous alloy particle reinforced composite (30 N).

the presence of amorphous/glassy particles. The improved wear/friction characteristics of the composite is attributed to: (i) uniform distribution of the amorphous alloy reinforcement particles, (ii) increased hardness, (iii) increased strength properties of the composite, (iv) metallic nature of the reinforcement and (v) intrinsically superior mechanical properties of $Ni_{60}Nb_{40}$ that ensures high load bearing capacity.

Representative SEM images showing the worn surfaces of unreinforced aluminium and Al-$Ni_{60}Nb_{40}$ composite are shown in Fig. 6. SEM images reveal adhesion as the wear mechanism in pure Al (Fig. 6a). Wear in the case of the composite does not occur by adhesion due to the presence of amorphous alloy particles. Rather, wear occurs by abrasion (scoring by the hard asperities of the steel counterface) (Fig. 6b).

Usually in composites containing ceramic reinforcements with size of the order of micrometer, third-body (debris) effect is severe during wear. The hard, ceramic micro-reinforcements present in the debris would cause counter-abrasion of the sliding surfaces, and would increase the wear rate. This is a major drawback in such composites, as the effect increases the overall wear rate and coefficient of friction[26-28]. In contrast, amorphous alloy when incorporated as reinforcement particles, does not seem to induce severe counter-abrasion due to their inherent metallic nature as they remain intact (bonded) with the matrix component of the wear debris (superior binding between metallic amorphous particle and metallic matrix).

4 Conclusions

Pure Al was incorporated with $Ni_{60}Nb_{40}$ amorphous alloy particle to produce Al-$Ni_{60}Nb_{40}$ amorphous particle reinforced composite using bi-directional

microwave-assisted rapid sintering. The conclusions are:

(i) Successful incorporation of $Ni_{60}Nb_{40}$ particles in Al-matrix was achieved by bi-directional microwave-assisted rapid sintering technique. The amorphous particle so reinforced show no matrix/particle incompatibility.

(ii) Microstructural features of the developed composite indicate: (i) no change in structural-state of the amorphous particle reinforcement, (ii) reinforcement being uniformly distributed (iii) clear interface, without undesirable reaction products. The effectiveness of the rapid sintering process in fabricating these novel composites is brough forth.

(iii) The Al-amorphous alloy particle composite exhibited significantly high strength properties in terms microhardenss, tensile strength and compression strength, coupled with no appreciable loss in tensile elongation as well as compressive ductility.

(iv) The strengthening mechanisms that contribute towards the superior performance of the synthesized composites are: (i) the intrinsically high mechanical properties of $Ni_{60}Nb_{40}$ and (ii) superior interfacial properties between matrix and reinforcement.

(v) The addition of amorphous reinforcement reduced the wear rate and friction coefficient. Third-body counter-abrasion has not been observed in the developed Al-$Ni_{60}Nb_{40}$ amorphous alloy particle reinforced composite, which is major advantage when compared to conventional ceramic reinforced composites.

(vi) The current work demonstrates that amorphous alloy/metallic glass particle as reinforcements in Al-

matrices can be very effective in improving the strength properties and can prove as superior substitutes when compared to the traditionally used ceramic reinforcements.

Acknowledgment

References

1 Miracle D B, *Comp Sci Tech*, 65 (2005) 2526.
2 Nair S V, Tien J K & Bates R C, *Intl Metals Rev*, 30 (1985) 275.
3 Thirumalvalavan S & Senthilkumar N, *Indian J Eng Mater Sci*, 26 (2019) 59.
4 Jailani, H, Rajadurai A, Mohan B & Sornakumar T, *Indian J Eng Mater Sci*, 22 (2015) 414.
5 Suryanarayana C & Inoue A, Bulk Amorphous Alloys (CRC Press, New York) 1st Edn, ISBN: 978-1-4200-8596-9, p.7.
6 Lee M, Bae D H, Kim W T & Kim D H, *Mater Trans*, 44 (2003) 2084.
7 Lee M H, Kim J H, Park J S, Kim J C, Kim W T & Kim D H, *Scripta Mater*, 50 (2004) 1367.
8 Scudino S, Liu G, Prashanth K G, Bartusch B, Surreddi B, Murty B S & Eckert J, *Acta Mater*, 57 (2009) 2029.
9 Kim J Y, Scudino S, Kühn U, Kim B S, Lee M H & Eckert J, *Metals*, 2 (2012) 79.
10 Dudina D V, Georgarakis K, Li Y, Aljerf M, LeMoulec A, Yavari A R & Inoue A, *Comp Sci Tech*, 69 (2009) 2734.
11 Dudina D V, Georgarakis K, Aljerf M, Li Y, Braccini M, Yavari A R & Inoue A, *Compost-A*, 41 (2010) 1551.
12 Aljerf M, Georgarakis K, Louzguine-Luzgin D, Le Moulec A, Inoue A & Yavari A R, *Mater Sci Eng A*, 532 (2012) 325.
13 Gupta M & Wong E, Microwaves and Metals (John Wiley & Sons, Singapore),1stEdn, ISBN: 978-0-470-82272-2, 2007, p.49.
14 Gupta M & Wong E, *Scripta Mater*, 52 (2005) 479.
15 Jayalakshmi S, Sahu, S Sankaranarayanan S, Gupta S & Gupta M, *Mater Des,* 53 (2014) 849.
16 Jayalakshmi S, Gupta S, Sankaranarayanan S, Sahu, S & Gupta M, *Mater Sci Eng A,* 581 (2013) 119.
17 Jayalakshmi, S & Gupta M, Metallic Amorphous Alloy Reinforcements in Light Metal Matrices (Springer Briefs in Materials, Springer, New York), 1st Edn, ISBN:97 8-3-319-15015-4, 2015, p.99.
18 Jayalakshmi S, Singh A R & Gupta M, *Technol,* 6 (2018) 1.
19 Jayalakshmi S, Sankaranarayanan S & Gupta M, *Metals,* 5 (2015) 743.
20 Koch C C, Davin O B, Mckamy C G & Scarbrough J O, *Appl Phys Lett*, 43 (1983) 1017.
21 Nardone V C & Prewo K M, *Scripta Metall*, 20 (1986) 43.
22 Arsenault R J & Fisher R M, *Scripta Metall*, 17 (1983) 67.
23 Chawla K K & Chawla N, Metal Matrix Composites (John Wiley & Sons, USA),1st Edn, ISBN: 100-387-23306-7, 2004, p.219.
24 Archard J, *J Appl Phys*, 24 (1953) 981.
25 Arvind Singh R, Jayalakshmi S, Sankaranarayanan S, Shabadi R, Konovalov S, Chen X Z & Gupta M, *Mater Today Proc*, 5 (2018), 16575.
26 Jayalakshmi S, Kailas S V, Seshan S & Fleury E, *J Mater Sci*, 41 (2006) 3743.
27 Jayalakshmi S, Kailas S V & Seshan S, *J Mater Sci*, 38 (2003) 1383.
28 Sannino A P & Rack H J, *Wear*, 189 (1995) 1.